

Supplemental Information

Molecular trick to reverse S_N2 step in a haloalkane dehalogenase

Martin Toul^{1,2,#}, Sergio M. Marques^{1,2,#}, Tadeja Gao^{1,2,#}, Hana Bernhardova^{1,2,#}, Ondrej Vavra^{1,2},
Veronika Novakova^{1,2}, Jiri Damborsky^{1,2}, David Bednar^{1,2,*}, Zbynek Prokop^{1,2,*}, Martin Marek^{1,2,*}

These authors contributed equally, * corresponding authors;

Correspondence: David Bednar (222755@mail.muni.cz); Zbynek Prokop (zbynek@chemi.muni.cz);
and Martin Marek (martin.marek@recetox.muni.cz)

¹ Loschmidt Laboratories, Department of Experimental Biology and RECETOX, Faculty of Science,
Masaryk University, Kamenice 5, 625 00 Brno, Czech Republic; ² International Clinical Research Center,
St. Anne's University Hospital Brno, Pekarska 53, 656 91 Brno, Czech Republic

Table S1: Comparison of kinetic constants obtained for LinB haloalkane dehalogenase variants. Kinetic constants were obtained after mixing the chloride anion (Cl^-) product or the 1-chlorohexane substrate ligands with LinB-wt, LinB-H272F, or LinB-H272N at either pH 7.5 or 10.5. All the experiments were performed in 100 mM glycine at 27 °C (300 K). The values are represented as best fit values \pm standard error values (95 % confidence intervals) based on nonlinear curve fitting. The details of kinetic data analysis are provided in **Supplementary Note 1**. n. a. = not applicable

	$K_d (\text{Cl}^-)$ [mM]	K_s [μM]	k_{+2} [s^{-1}]	k_{-2} [s^{-1}]	$K_{+2} (k_{+2}/k_{-2})$ [-]
LinB-wt (pH 7.5)	620 ± 160 (353–1192)	90 ± 10 (60–140)	84 ± 3 (74–88)	33 ± 1 (28–39)	2.55 ± 0.12
LinB-wt (pH 10.5)	470 ± 80 (320–720)	180 ± 20 (90–370)	63 ± 1 (57–74)	33 ± 1 (27–42)	1.91 ± 0.07
LinB-H272F (pH 7.5)	340 ± 80 (190–650)	540 ± 80 (280–1150)	0.025 ± 0.002 (0.019–0.033)	0.074 ± 0.001 (0.072–0.076)	0.34 ± 0.03
LinB-H272F (pH 10.5)	250 ± 60 (150–450)	250 ± 40^a (80–610)	0.069 ± 0.037^a (0.027–0.148)	0.137 ± 0.075^a (0.024–0.267)	0.50 ± 0.39
LinB-H272N (pH 7.5)	370 ± 140 (140–1100)	320 ± 70 (210–510)	6.8 ± 0.4 (5.9–7.8)	0.007 ± 0.006 (0.000–0.295)	1010 ± 520
LinB-H272N (pH 10.5)	240 ± 70 (110–610)	690 ± 110 (180–5540)	< 0.01	< 0.01	n. a.

^a The values of these parameters were derived from global numerical fitting of kinetic data as described in Supplementary Note 1 so compared to 95 % confidence intervals provided for other parameters, the values in brackets for these three parameters correspond to the lower and upper bound limits after setting the χ^2/χ^2_{\min} threshold to 0.95. Cross correlation analysis of these three parameters is provided in Figure S18.

Table S2: Crystallographic data collection and refinement statistics.

Data collection*	LinB-H272F
Wavelength (Å)	1
Space group	<i>P2₁2₁2₁</i>
Cell dimensions	
a, b, c (Å)	51.496, 65.448, 90.171
α , β , γ (°)	90, 90, 90
Resolution (Å)	44.17 – 1.55 (1.61 – 1.55)
Total reflections	586,446 (56,284)
Unique reflections	44,614 (4,309)
Rmerge	18.0 (160.1)
I / σ I	11.71 (1.47)
Completeness (%)	99.4 (97.6)
Multiplicity	13.1 (13.1)
CC(1/2)	99.8 (70.1)
Wilson B-factor	13.09
Refinement	
Resolution (Å)	44.172 – 1.551 (1.607 – 1.551)
No. reflections	44,614 (4,309)
Rwork (%) / Rfree (%)	17.41 / 20.13
Number of atoms	
Protein	2,390
Ligand	102
Water	246
B-factors	
Protein	14.6
Ligand	29.5
Water	26.7
R.m.s deviations	
Bond lengths (Å)	0.007
Bond angles (°)	0.96
Ramachandran favoured (%)	96.23
Ramachandran allowed (%)	3.77
Ramachandran outliers (%)	0
PDB ID code	7NFZ

*Values in parentheses are for the highest-resolution shell.

Table S3: Residues used for the setup of the ASMD simulations.

Protein	Tunnel	Steering residue
LinB-H272F	p1	Tyr 82
	p2	Pro 203
	p5	Ser 206
LinB-H272N	p1	Leu 89
	p2	Met 21
	p5	Arg 201
LinB-wt	p1	Tyr 82
	p2	Arg85
	p5	Glu 161

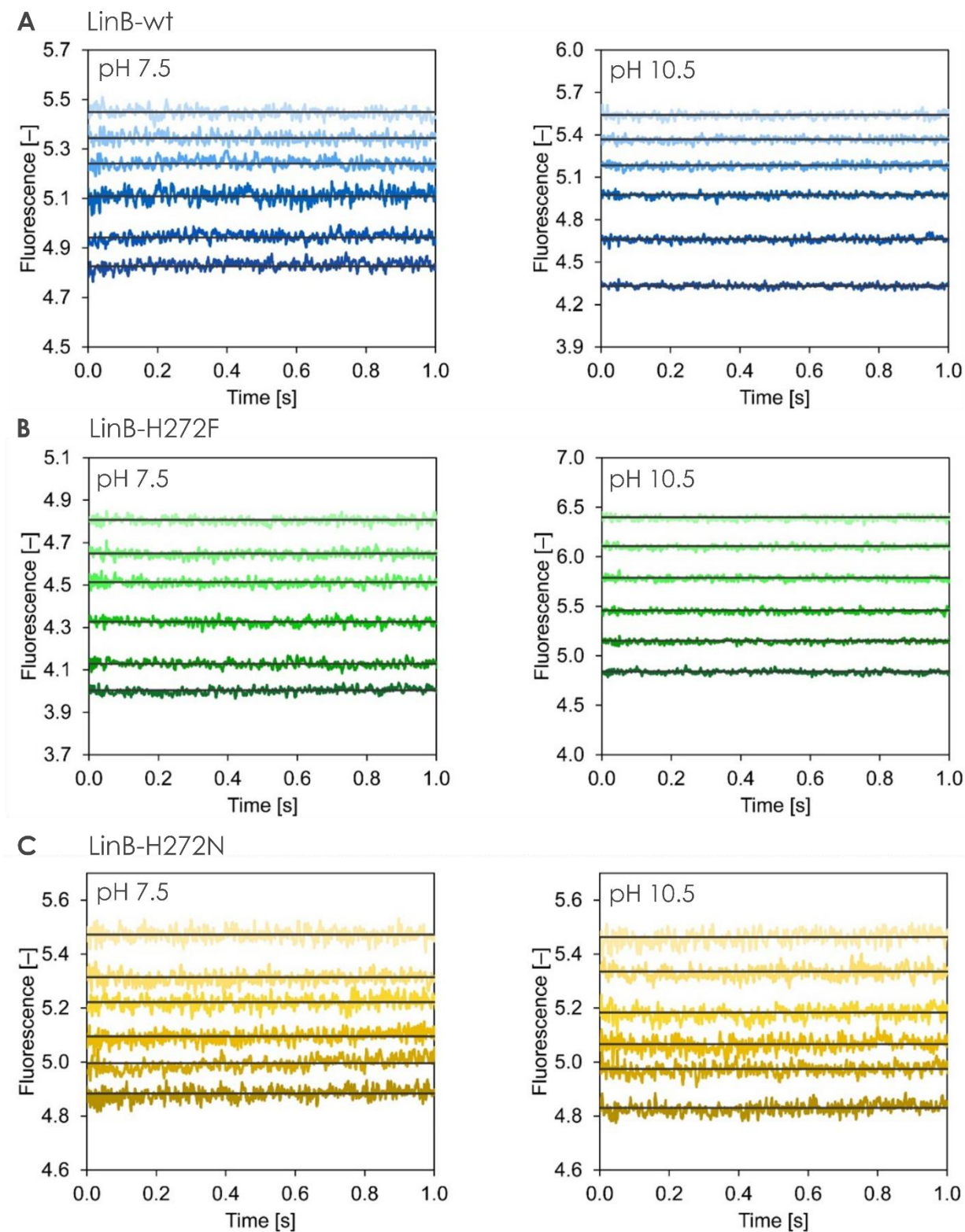


Figure S1: Kinetic traces of Cl⁻ binding to LinB variants: LinB-wt (A), LinB-H272F (B), and LinB-H272N (C), at pH 7.5 (left) and pH 10.5 (right). Solid lines represent the best fit. The concentration range of Cl⁻ during the measurements was between 0 and 2000 mM. All the experiments were performed in 100 mM glycine at 27 °C (300 K).

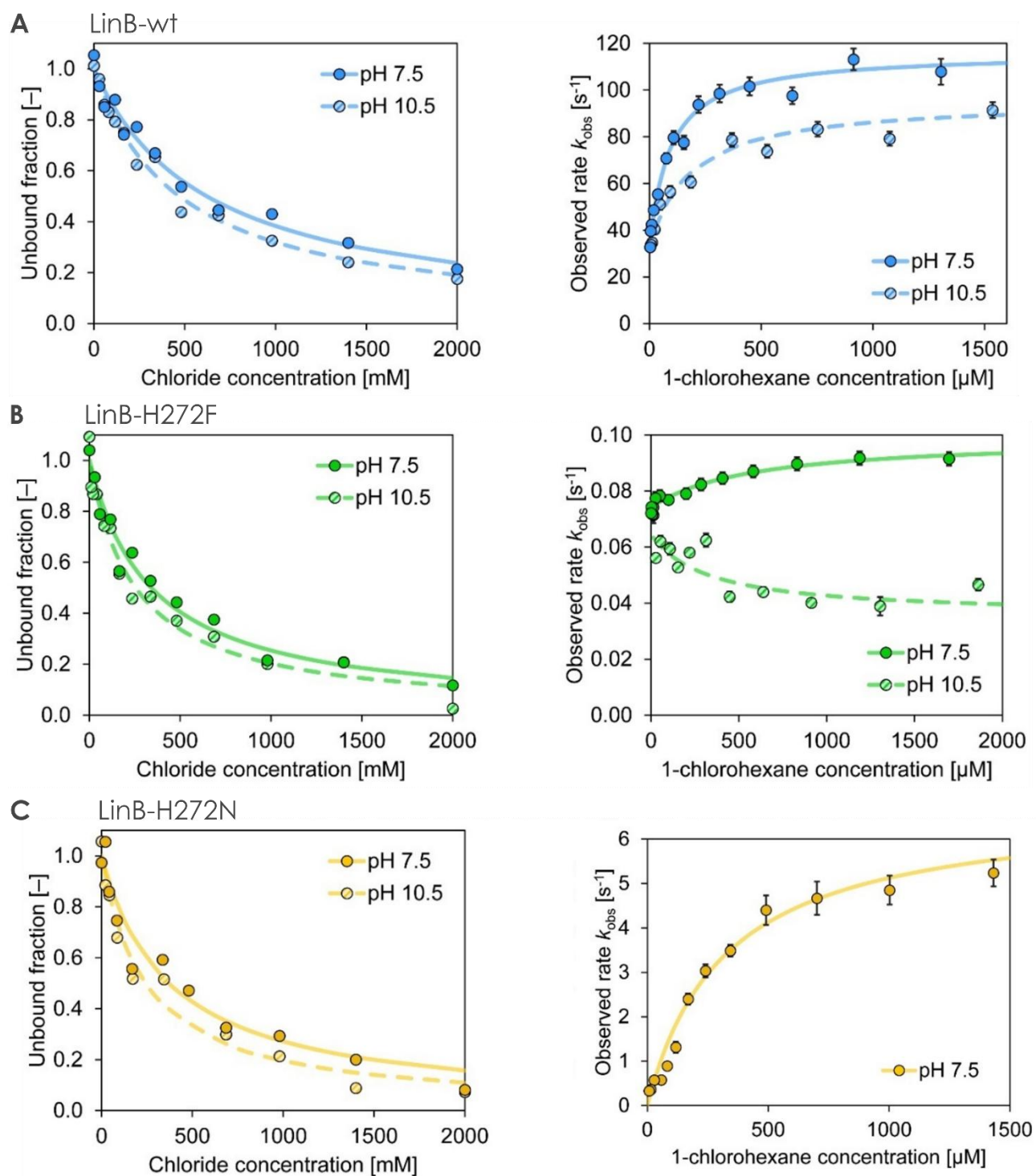


Figure S2: Transient kinetic analysis of Cl^- (left) and 1-chlorohexane (right) for all three LinB variants: LinB-wt (A), LinB-H272F (B), and LinB-H272N (C), at pH 7.5 (solid points) or pH 10.5 (hatched points). The analytical fitting of hyperbolic concentration dependencies was performed for equilibrium fluorescence levels upon Cl^- binding and for observed exponential rates, k_{obs} , of fluorescence decrease upon 1-chlorohexane binding and processing. Lines represent the best fit. The datapoints were extracted from kinetic data collected in 100 mM glycine at 27 °C (300 K).

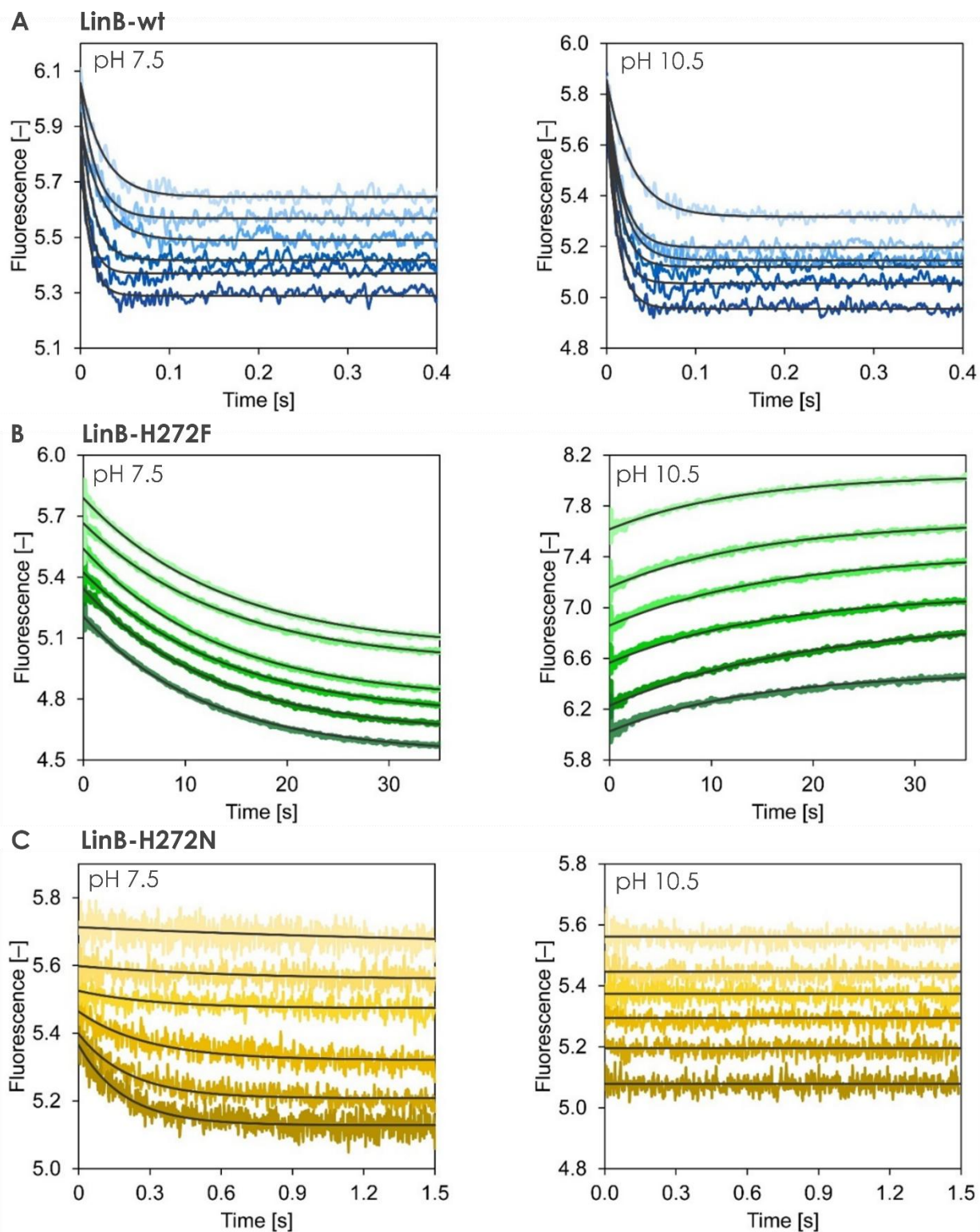


Figure S3: Kinetic traces after mixing 1-chlorohexane (substrate) with LinB variants: LinB-wt (A), LinB-H272F (B), and LinB-H272N (C), at pH 7.5 (left panels) and pH 10.5 (right panels). Solid lines represent the best fit. The concentration range of 1-chlorohexane during the measurements was between 0 and 1860 μM . All the experiments were performed in 100 mM glycine at 27 $^{\circ}\text{C}$ (300 K).

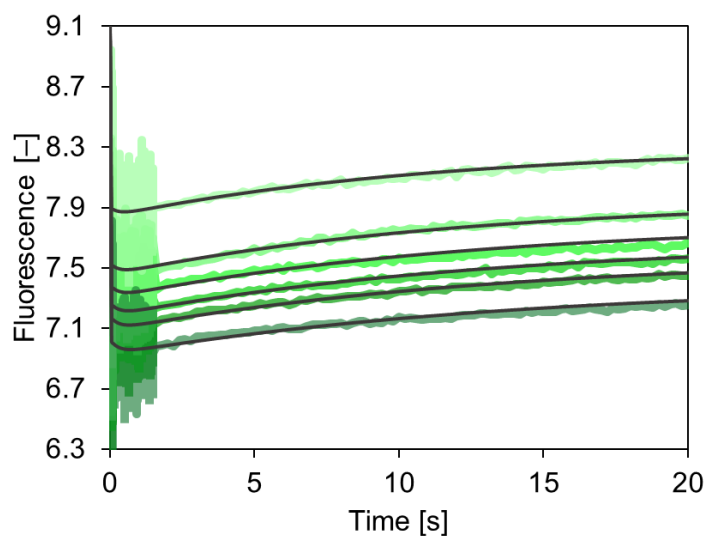


Figure S4: Numerical fitting of the LinB-H272F kinetic data upon mixing with 1-chlorohexane at pH 10.5. Due to the complex behaviour of the mutant at higher pH, including the conformational selection binding mechanism and chloride release after the alkyl-enzyme intermediate formation, numerical data analysis was required. The final fit (solid lines) could adequately account for all the untypical experimental observations, supporting the proposed extended model. The experiment was performed in 100 mM glycine at 27 °C (300 K).

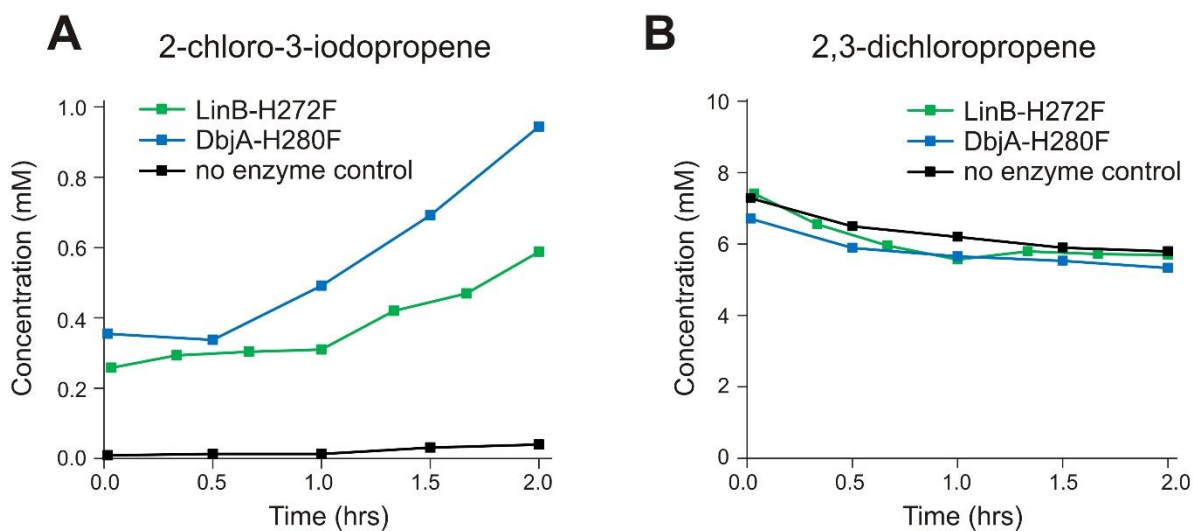


Figure S5: Transhalogenation reaction catalyzed by LinB-H272F and DbjA-H280F dehalogenases. Formation of the transhalogenation product 3-iodo-2-chloropropene (A) from the substrate 2,3-dichloropropene (B) in the presence of 100 mM iodide, catalyzed by LinB-H272F (green) and DbjA-H280F (blue). The no-enzyme reaction is shown as a control (black).

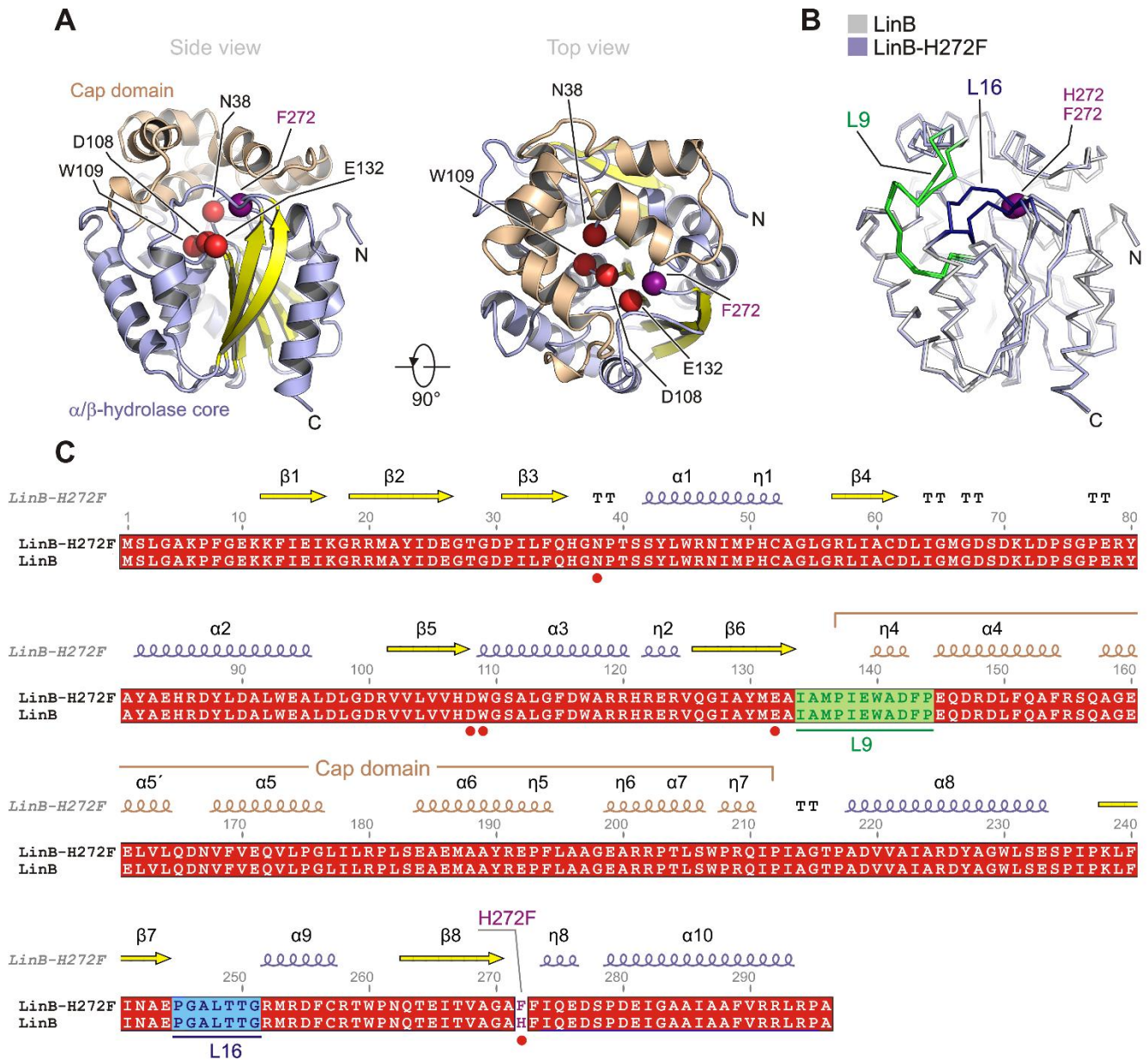


Figure S6: Overall structure of LinB-H272F. (A). Cartoon representation of LinB-H272F. Catalytic pentad residues are shown as red spheres, with the exception of introduced F272 that is colored violet. The central 8-stranded sheet is colored yellow, the helical cap domain is colored wheat, the remaining parts are colored light-blue. (B) Ribbon representation of structural comparison between LinB-wt (grey) and LinB-H272F (light-blue). The L9 loop is colored green, and the L16 loop is colored dark-blue. Note that major structural deviations are made by both L9 and L16 loops. (C) Sequence alignment between LinB-H272F and LinB-wt. Topology of secondary structure elements is denoted above the alignment.

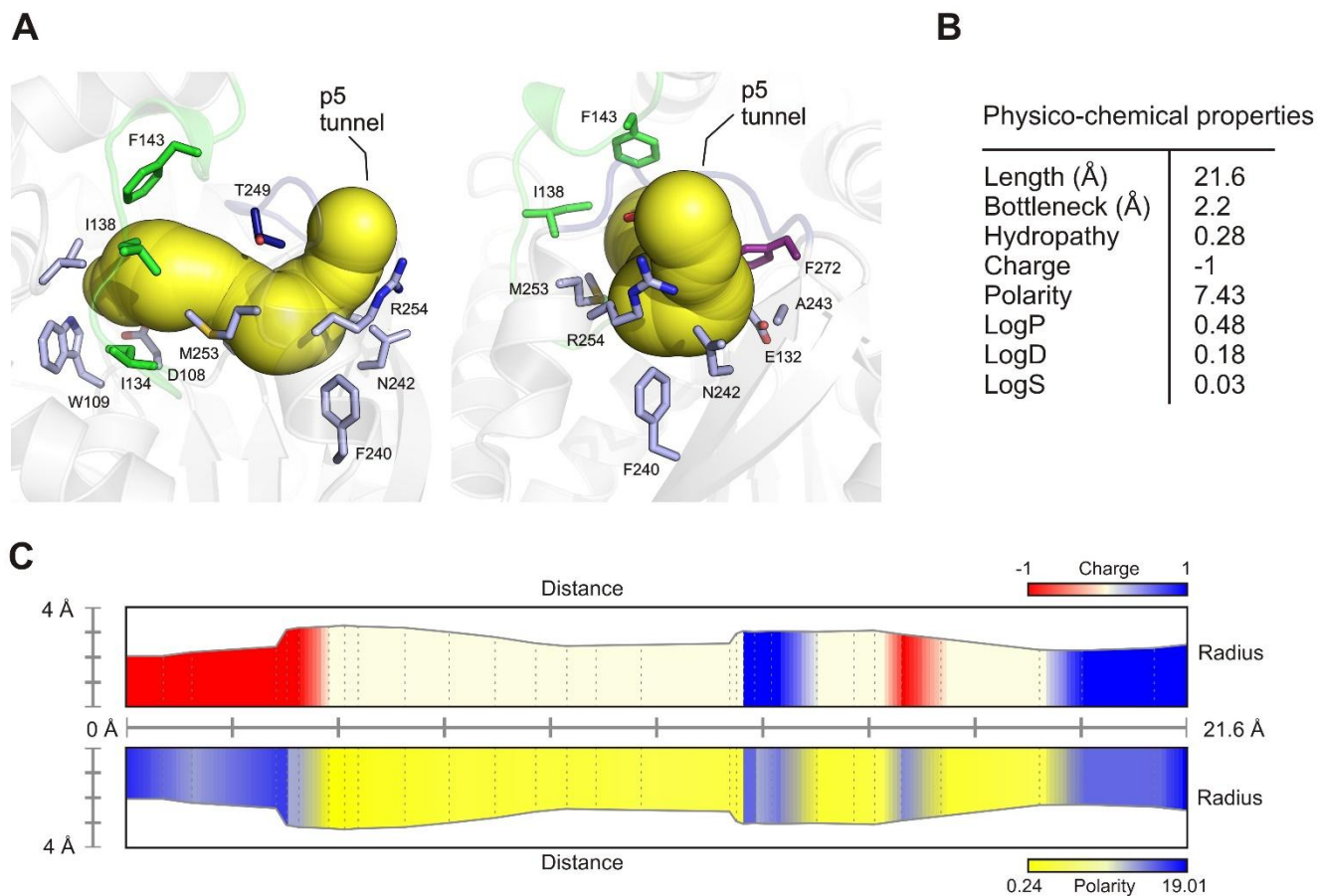


Figure S7: Analysis of the p5 tunnel in LinB-H272F. (A) Identification of visualization of p5 tunnel (yellow) by MOLE software tool.¹ Amino acids surrounding the tunnel are shown as sticks. (B) Table with physico-chemical properties of the p5 tunnel. (C) The charge and hydrophobicity properties of the p5 tunnel.

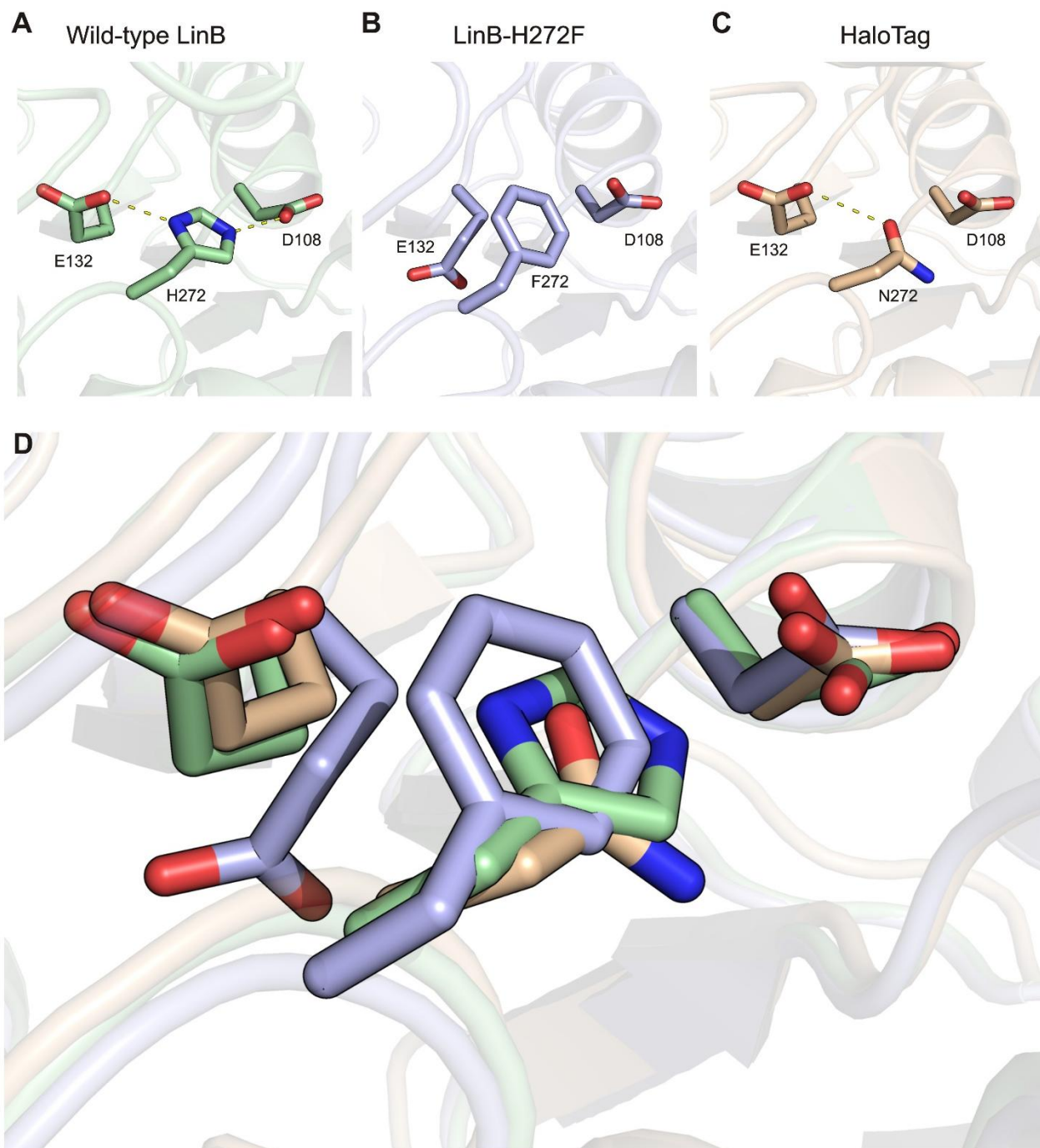


Figure S8: Structural comparison between LinB, LinB-H272F and HaloTag proteins. The positioning of catalytic triad residues (proton-relay system) in LinB-wt (A), LinB-H272F (B), and HaloTag (C). Note that a catalytic acid (E132) is flipped-out from its canonical position in LinB-H272F. (D) Superposition of all structures. LinB-wt (lightgreen), LinB-H272F (lightblue), and HaloTag (wheat).

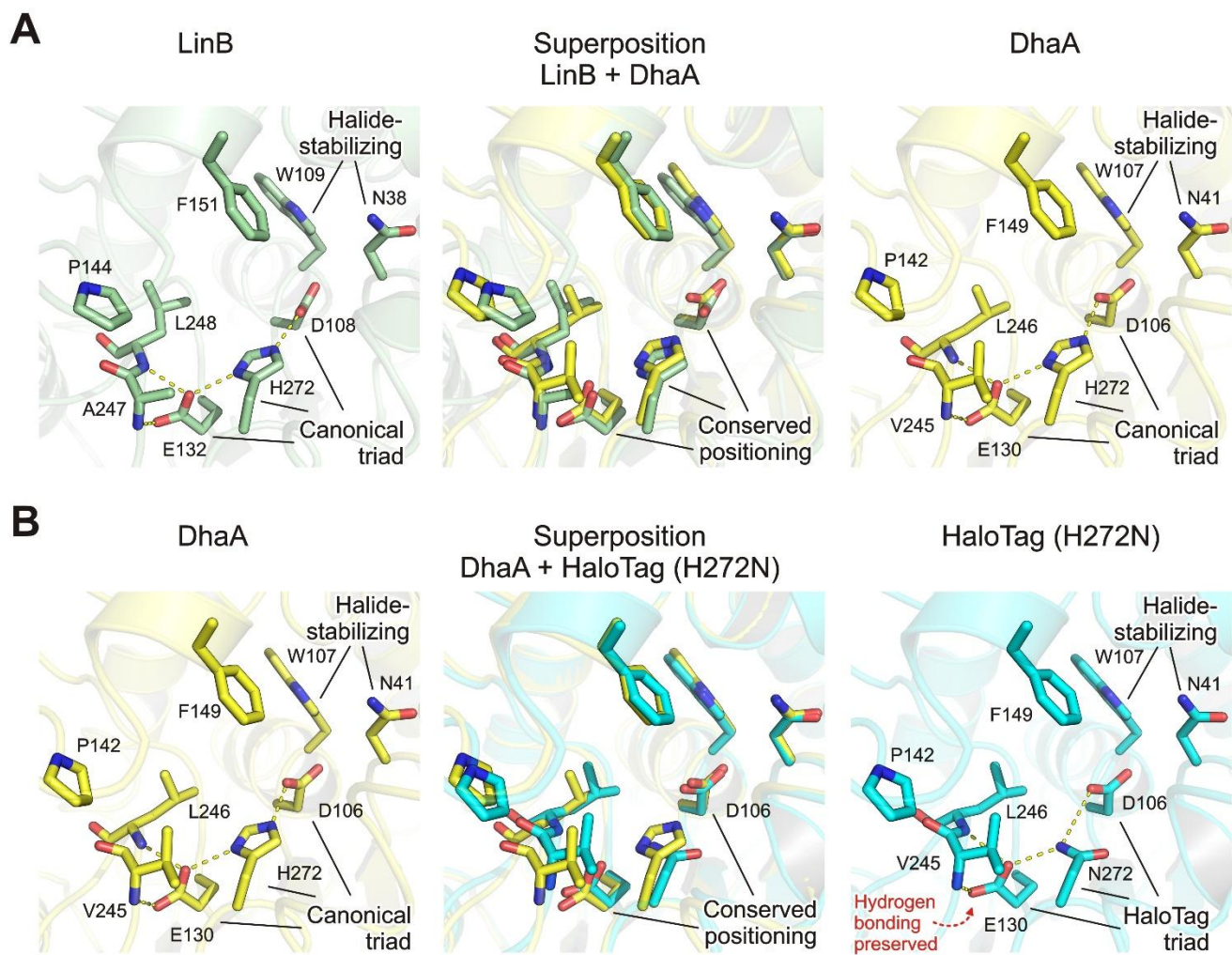


Figure S9: Structural superpositions of catalytic triad residues (proton-relay system) and surroundings residues between LinB and DhaA (A), and DhaA and HaloTag (H272N) (B). Note that the positioning of catalytic triads, L16 loop residues (L248 and L246, respectively), and the corresponding hydrogen bonding in LinB and DhaA is identical (A). The same is true when comparing DhaA and HaloTag (H272N), demonstrating that the presence of the asparagine (H272N) does not disturb the hydrogen bonding interactions between the catalytic triad and the surrounding L16 loop.

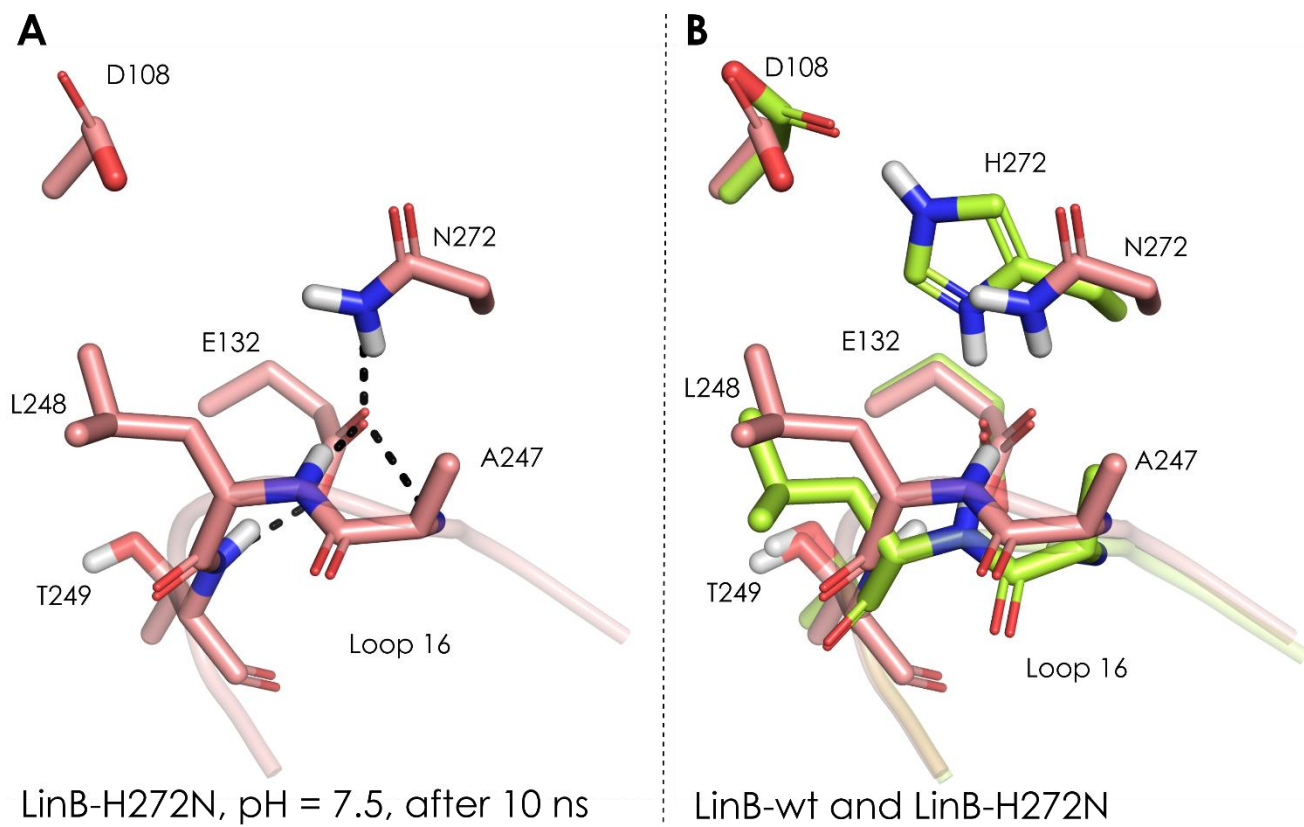


Figure S10: LinB-H272N after 10 ns of MD simulations. A: D108 conformation changes compared to the initial Rosetta model (see **Figure 5D** of the main article), resulting in the loss of the H-bond between D108 and N272. B: Superimposition of LinB-wt and LinB-H272N.

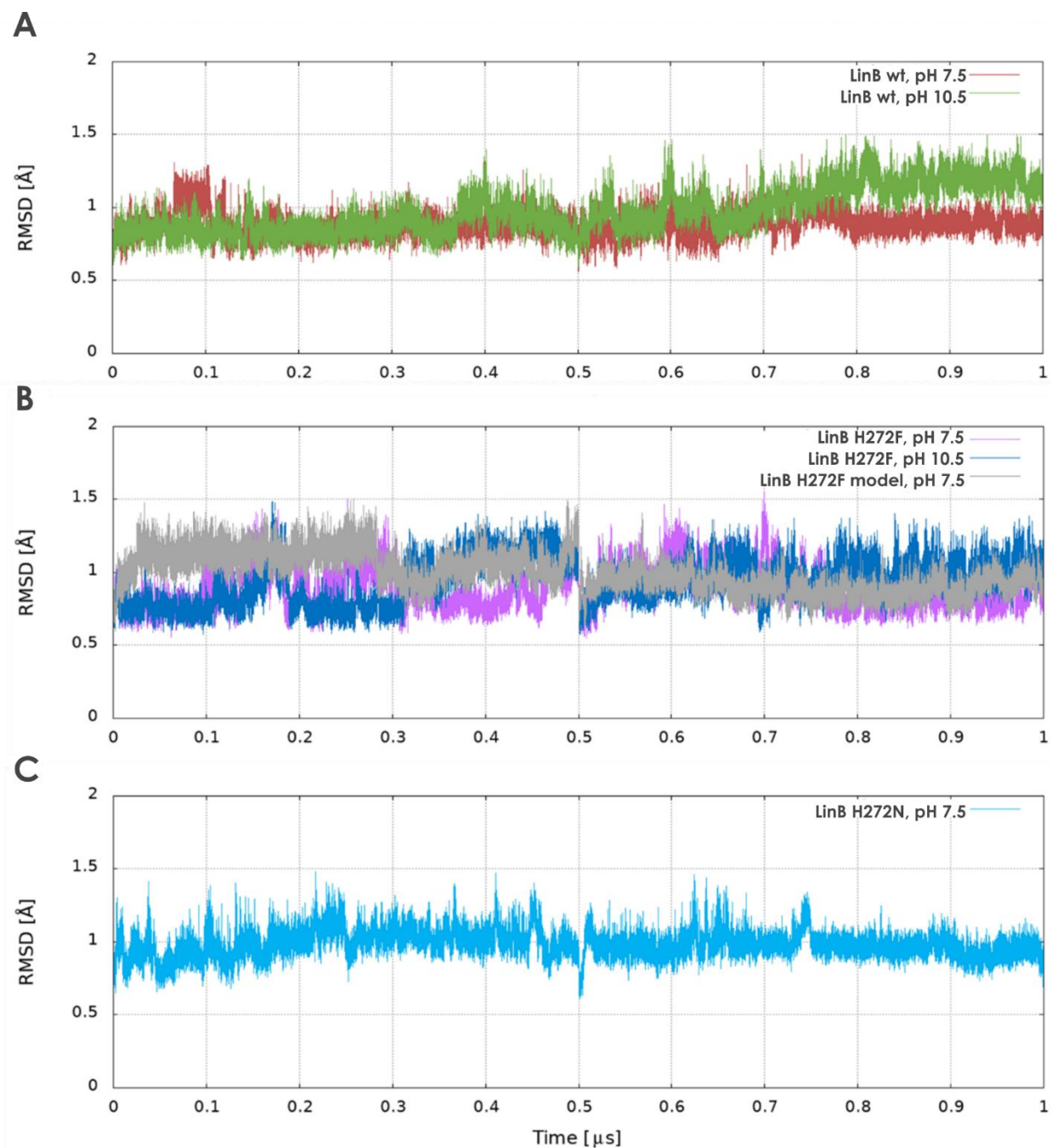


Figure S11: Variation of the root-mean-square deviation (RMSD) of the backbone atoms during the MD simulations with respect to the initial structures, for the different systems at different pH values. A: LinB-wt, B: LinB-H272F (started from the crystal structure and the *in silico* model), C: LinB-H272N (pH 7.5). Two independent MD simulations were performed for every protein, each one consisting of 500 ns. Here, they are presented sequentially. The plateaus observed at the final portion of every MD, together with the low RMSD values, below 1.5 Å, confirm their stability.

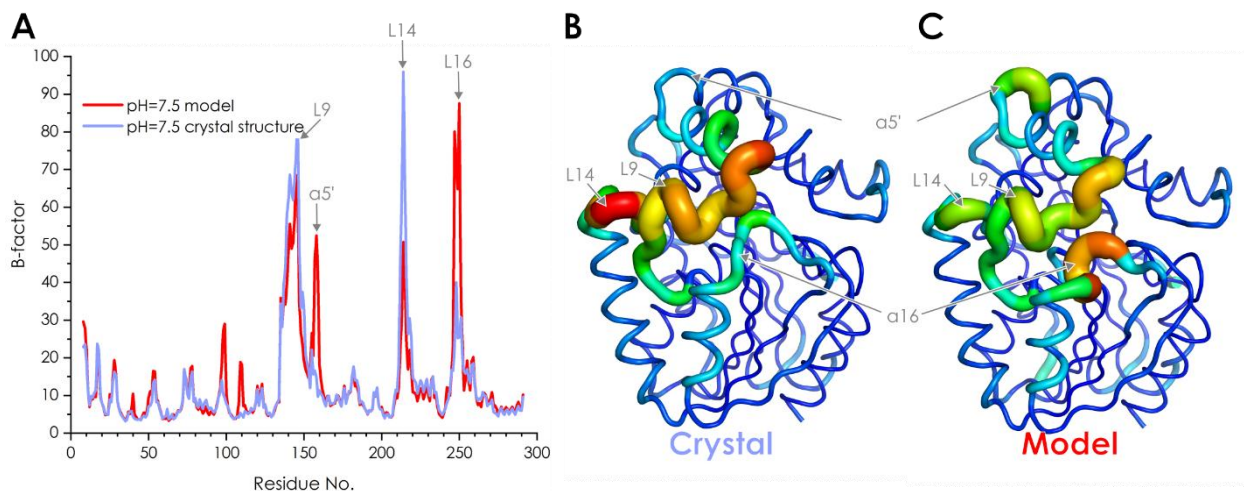


Figure S12: B-factor values during MD simulations of LinB-H272F at pH 7.5. A: Graph representation of B-factor values of crystal structure (light blue) and model (red). B and C: Putty tubes representation of crystal and model structure, respectively. A hotter (redder) and thicker putty tube indicates higher B-factor (higher flexibility); the regions with more pronounced flexibility changes are indicated.

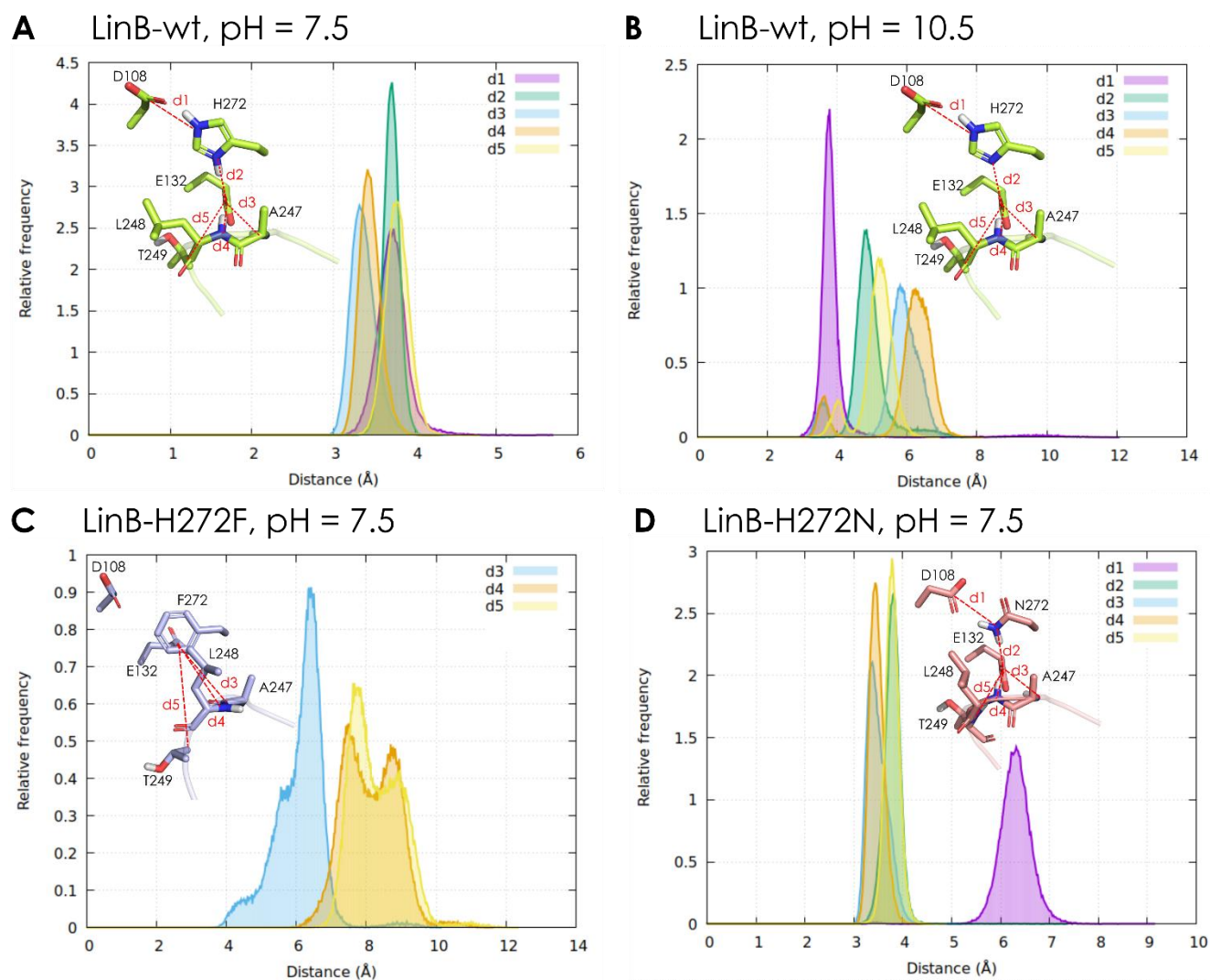


Figure S13: Distribution of interatomic distances during the MD simulations, representing the H-bond network shown in **Figure 5** of the main article. LinB-wt at pH 7.5 (A), LinB-wt at pH 10.5 (B), LinB-H272F at pH 7.5 (C), and LinB-H272N at pH 7.5 (D). The distance values of 3-4 Å correspond to H-bonds. The insets in each panel depict the nature of distances: (i) d1 (D108-C γ -H272-N ϵ for LinB-wt or D108-C γ -N272-N δ for LinB-H272N), (ii) d2 (E132-C δ -H272-N δ or E132-C δ -N272-N δ), (iii) d3 (E132-C δ -A247-N), (iv) d4 (E132-C δ -L248-N), and (v) d5 (E132-C δ -T249-N).

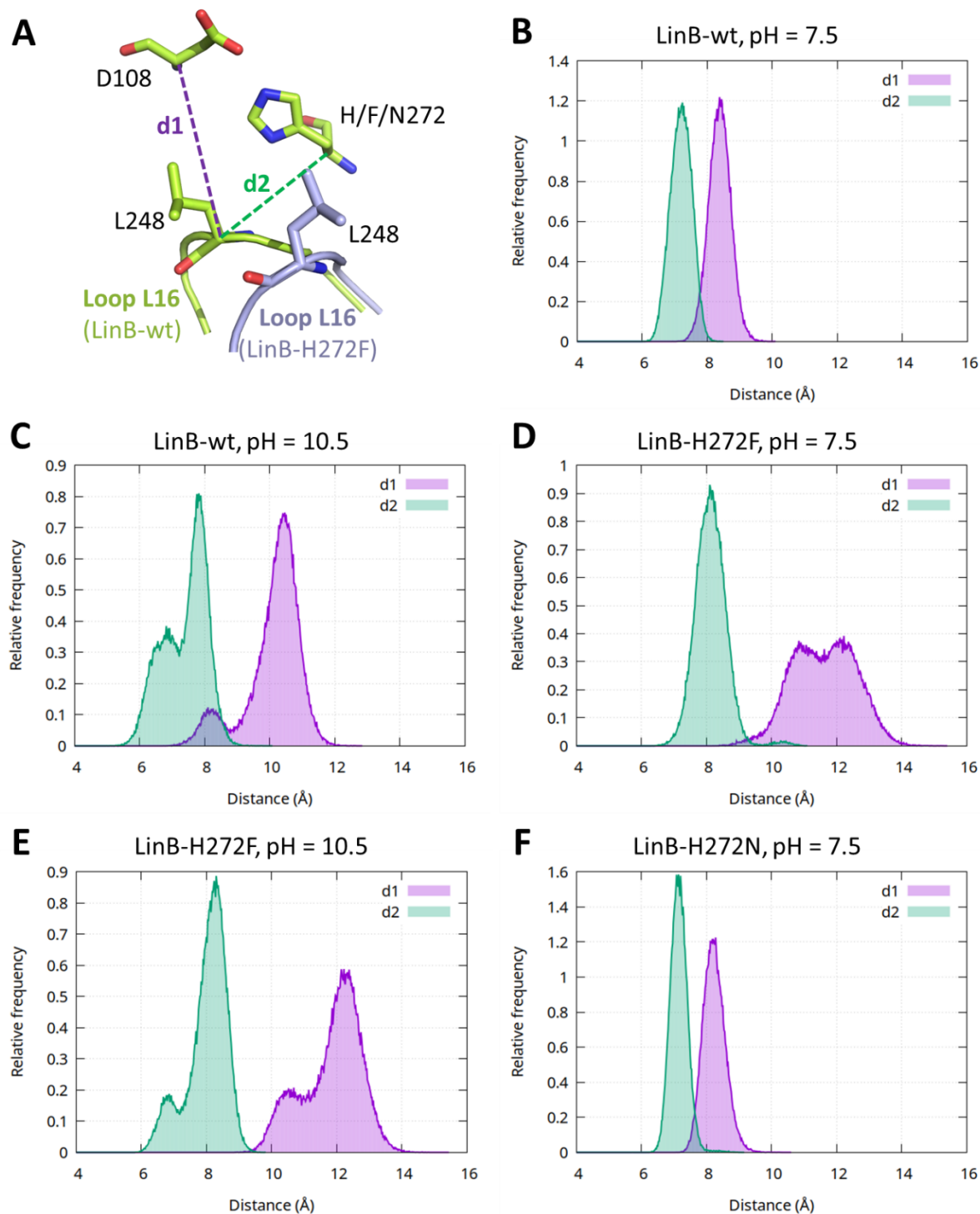


Figure S14: Distribution of interatomic distances during the MD simulations, representing the distances between loop L16 to two active site residues. Illustration of the distances reported, (d1) between the C α atoms of loop residue L248 and catalytic residue D108, and (d2) between residue L248 and mutated residue 272 (A). Distance distributions are presented for LinB-wt at pH 7.5 (B), LinB-wt at pH 10.5 (C), LinB-H272F at pH 7.5 (D), LinB-H272F at pH 10.5 (E), and LinB-H272N at pH 7.5 (F). In (A) LinB-wt is represented in light green and, for reference, loop L16 of LinB-H272F is shown in light blue.

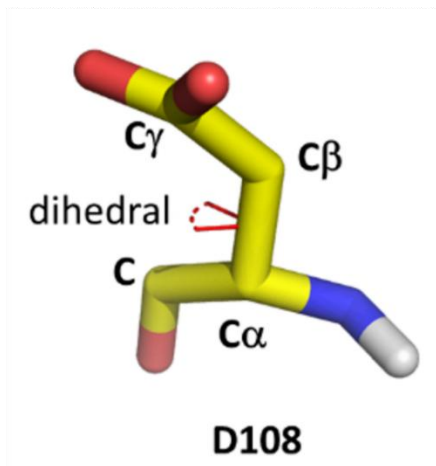
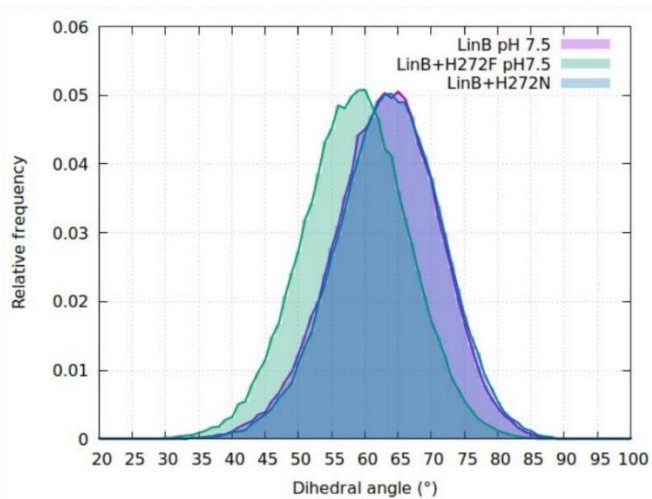
A**B**

Figure S15: Dihedral angle of the catalytic D108. A: The dihedral angle of D108 is defined as an angle between two planes. First plane consists of atoms C-C α -C β and the second plane consists of atoms C α -C β -C γ . The dihedral angle also corresponds to the rotation around the two atoms, C α and C β , as depicted in the figure. B: Distribution of the D108 dihedral angle in the MD simulations at pH 7.5 for LinB-wt (purple), LinB-H272F (green), and LinB-H272N (blue).

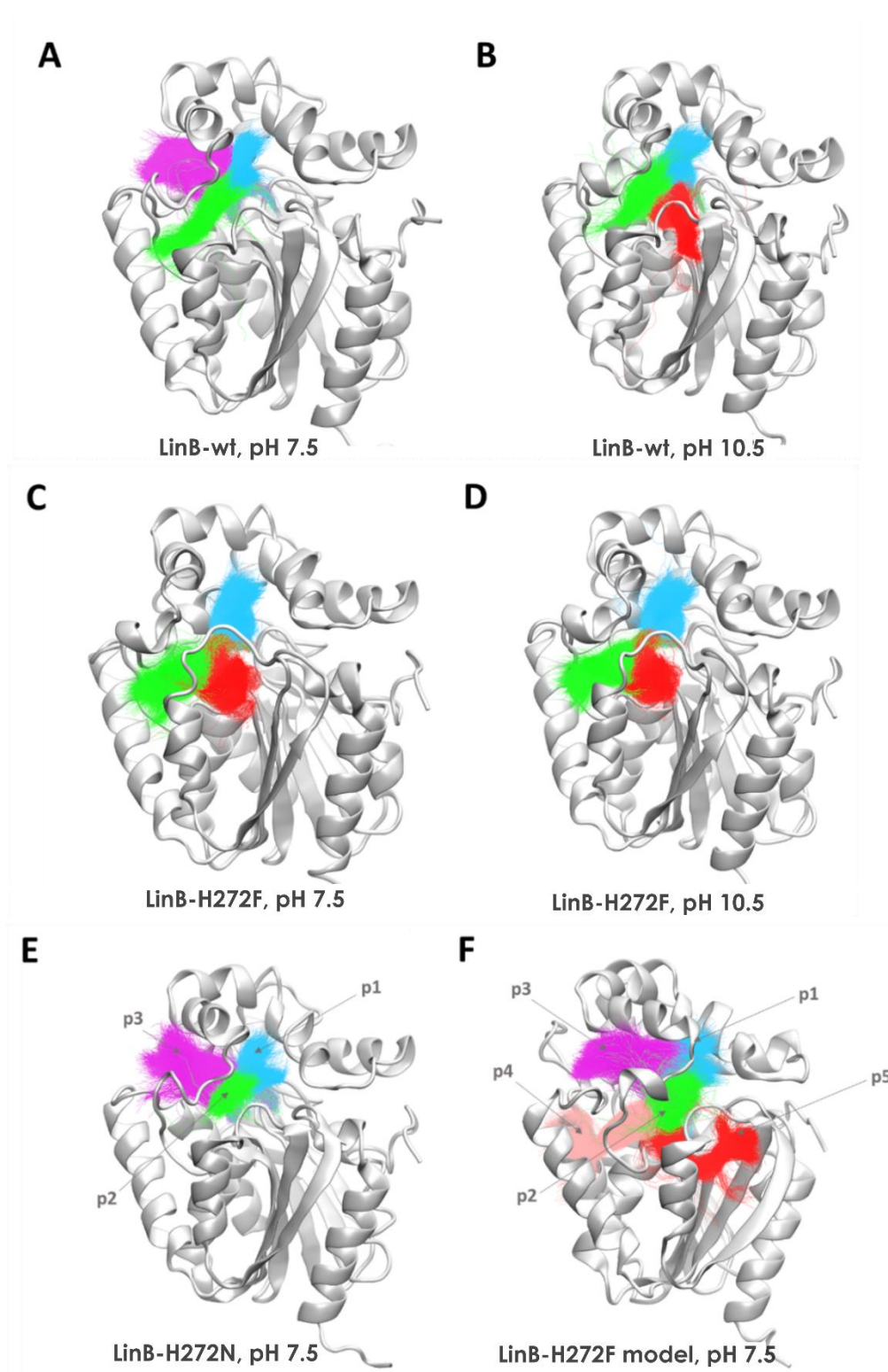


Figure S16: Access tunnels calculated in the combined MD simulations for LinB-wt (A and B), and LinB-H272F (C and D) at neutral (left) and alkaline (right) pH, LinB-H272N (E), and the *in silico* model of LinB-H272F (F) at pH 7.5. The tunnels are represented by the superimposed coloured lines, collected from the simulation snapshots, and clustered according to their topologies. p1 (cyan), p2 (slot tunnel, green), p3 (magenta), p4 (salmon) p5 (red).

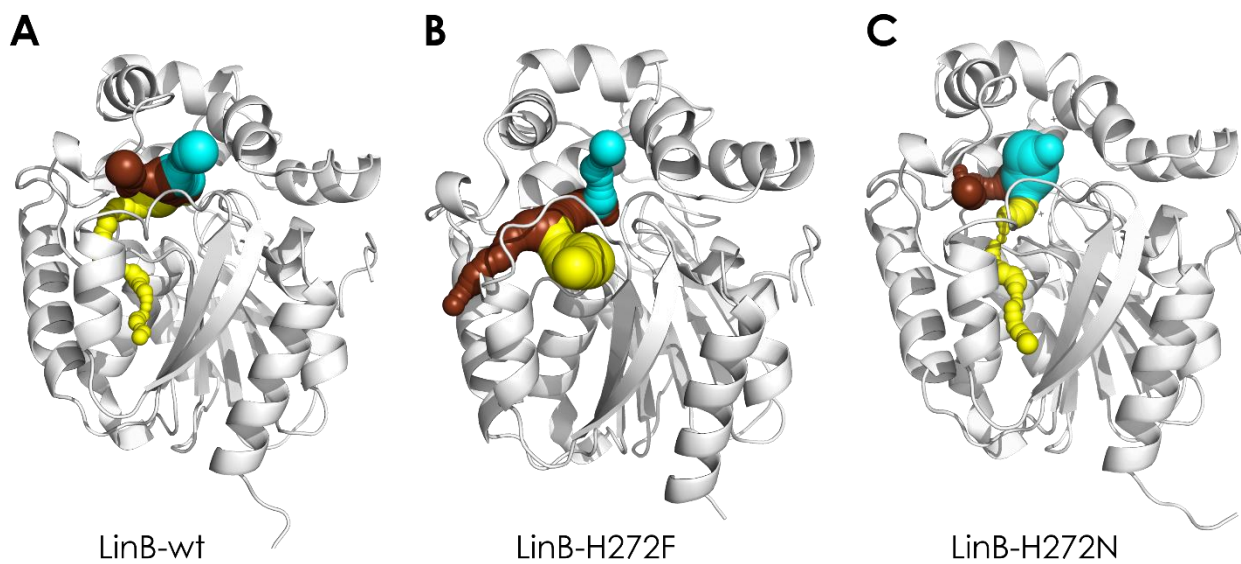


Figure S17: Structures of LinB variants with calculated tunnels using the probe with radius of 0.7 Å. LinB-wt (A), LinB-H272F (B), and LinB-H272N (C). p1 tunnel (cyan), p2 tunnel (brown), and p5 tunnel (yellow).

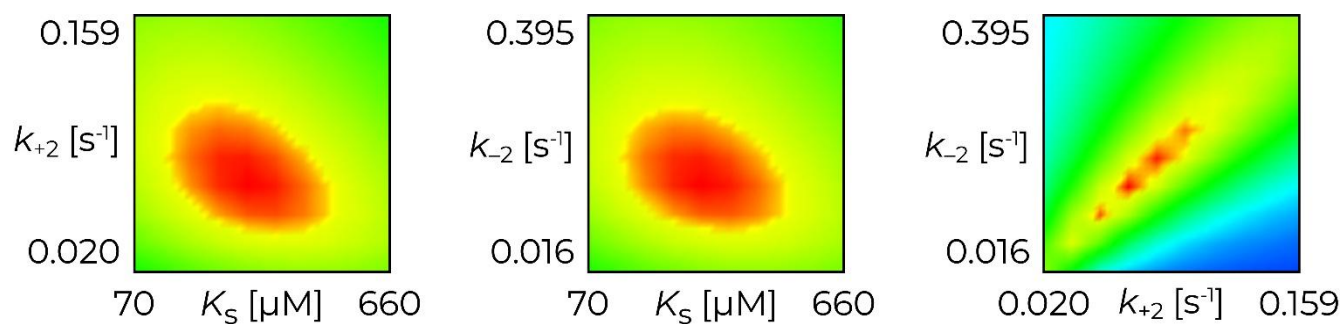


Figure S18: Confidence contour analysis of parameters obtained by global numerical simulation fitting of kinetic data collected for LinB-H272F at pH 10.5. The results were obtained by running the FitSpace 2D analysis in the KinTek Explorer software by setting the χ^2/χ^2_{\min} threshold to 0.95 after fixing other parameters that were not constrained enough (rate constants of potential ion release and conformational changes). Margin of the red area corresponds to the threshold of 0.95, providing well defined space and no cross-correlation of extracted parameters. The analysis is based on kinetic analysis of data provided in Figure S4.

Supplementary Note 1:

Kinetic analysis of 1-chlorohexane processing by LinB variants

Apart from the typical single-exponential decrease of fluorescence traces with the increasing hyperbolic concentration dependence of observed exponential rates k_{obs} (described in the Materials and Methods section), more complex and untypical kinetic data were collected in the case of histidine mutants LinB-H272F and LinB-H272N at the increased value of pH 10.5.

When LinB-H272F was mixed with 1-chlorohexane at increased pH of 10.5, (i) the fluorescence signal was unexpectedly increasing with time after a quick signal drop in the instrument dead-time, and furthermore, (ii) the concentration dependence of observed rates yielded a decreasing trend. The increase of the fluorescence signal and regeneration to the original level indicated that the chloride anion was released from the enzyme active site after the alkyl-enzyme intermediate was formed. This is unique in comparison with LinB-wt, other common haloalkane dehalogenases, and even LinB-H272F at physiological pH where the halide anion does not leave until the alkyl-enzyme intermediate is hydrolyzed and both the alcohol as well as the halide products are released.

The hyperbolic decrease of the observed rate with increasing substrate concentration pointed out the conformational selection mechanism of the substrate binding by LinB-H272F at pH 10.5. None of these two events has ever been observed previously in haloalkane dehalogenases and it is presumed that the untypical behavior might be due to the change of protonation states at alkaline pH causing a loss of important residue contacts and a newly formed tunnel which was detected in crystal structures and MD simulations of this variant. This extended model of substrate processing was tested by numerical simulation data fitting and a good fit, accounting for the unusual observations, could be obtained (**Figure S4**). This result supported the postulated hypothesis, but further experiments would be needed to fully confirm the suggested mechanism.

Finally, the kinetics of 1-chlorohexane processing by LinB-H272N was also affected by the increased pH environment. Fluorescence traces exhibited no significant decrease within the experimental time window of 100 seconds, suggesting highly impaired kinetics with the values of exponential observed rates lower than 0.01 s^{-1} . This value set the upper limit for both the forward and reverse rate constants of the alkyl-enzyme intermediate formation (k_{+2} and k_{-2}) without a possibility to determine exact values which were too slow to be derived from the obtained kinetic traces. The value of the substrate binding dissociation constant K_s was derived based on the concentration dependence analysis of the drop of the initial fluorescence level caused by the bound substrate, showing a typical hyperbolic dependence.

References

1. Pravda, L., Sehnal, D., Tousek, D., Navratilova, V., Bazgier, V., Berka, K., Svobodova Varekova, R., Koca, J., Otyepka, M. (2018). MOLEonline: a web-based tool for analyzing channels, tunnels and pores (2018 update). *Nucleic Acids Res.* 46 (W1), W368-W373.